

UNCLASSIFIED

AD **4 6 4 3 1 4**

DEFENSE DOCUMENTATION CENTER

FOR

SCIENTIFIC AND TECHNICAL INFORMATION

CAMERON STATION ALEXANDRIA, VIRGINIA



UNCLASSIFIED

NOTICE: When government or other drawings, specifications or other data are used for any purpose other than in connection with a definitely related government procurement operation, the U. S. Government thereby incurs no responsibility, nor any obligation whatsoever; and the fact that the Government may have formulated, furnished, or in any way supplied the said drawings, specifications, or other data is not to be regarded by implication or otherwise as in any manner licensing the holder or any other person or corporation, or conveying any rights or permission to manufacture, use or sell any patented invention that may in any way be related thereto.

⑤ Yale Univ. [redacted] New Haven, Conn.
School of Engineering.

①

~~Department of Engineering and Applied Sciences~~

MAIL ADDRESS: Mason Laboratory
400 Temple Street

AD NO. 464314
FILE COPY

⑪ MAR 21 1965

⑥ WEAK WAVES IN RELAXING FLOWS ,

⑩ by Peter P. Wegener, Boa-Teh Chu and W. A. Klikoff, Jr.

⑮

[redacted] Contract Nonr 609(46)
"Experimental and Analytical Study of Nonequilibrium
Flow Phenomena." This research is part of Project
DEFENDER under the joint sponsorship of the Advanced
Research Projects Agency, Department of Defense, and
the Office of Naval Research, Fluid Dynamics Branch.
Submitted by Peter P. Wegener, Principal Investigator.

DDC
MAY 28 1965
DDC-IRA E

* Now with Sandia Corporation, Albuquerque, New Mexico.

464314


2


2 March 1965

Weak waves in relaxing flows*

by

Peter P. Wegener, Boa-Teh Chu and W. A. Klikoff, Jr.**

 Theoretical and experimental investigations are described of the linearized wave equation of supersonic flow with a single relaxation process. Firing range experiments using a known model gas mixture with a single relaxation process are discussed. Qualitatively, it is shown that weak conical and spherical waves decay as predicted by theory. In addition, this decay can be determined quantitatively for conical disturbances; and, satisfactory agreement with theory is found. For application to unknown relaxation processes, it is suggested that observation of the damping of weak waves provides an additional tool for the study of fast rate processes.



* This research is part of Project DEFENDER under the joint sponsorship of the Advanced Research Projects Agency, Department of Defense, and the Office of Naval Research, Fluid Dynamics Branch.

** Now with Sandia Corporation, Albuquerque, New Mexico.

1. Introduction

In treating relaxing flows with one nonequilibrium mode a rate equation for a progress variable, q , needs to be considered. With p , ρ , τ denoting the pressure, density, and a relaxation time of the medium, we have

$$\frac{Dq}{Dt} = \frac{L(p, \rho, q)}{\tau}, \quad (1)$$

where L is a function of the thermodynamic state of the medium and $L[p, \rho, \bar{q}(p, \rho)] \equiv 0$, with \bar{q} being the progress variable at equilibrium. For small-disturbances, equation (1) may be linearized and written as

$$\frac{Dq}{Dt} = -v(q - \bar{q}) \quad (1')$$

with a rate constant defined by $v = -\frac{\partial L}{\partial q}/\tau$. The equation for the propagation of small-disturbances linearized about the state of thermodynamic equilibrium and incorporating a rate equation like equation (1') is well-known (see Moore 1958 or Clarke 1964.) In terms of the velocity perturbation potential, ϕ , we have

$$\tau_0 \frac{\partial}{\partial t} \left(\frac{1}{a_f^2} \phi_{tt} - \nabla^2 \phi \right) + \left(\frac{1}{a_e^2} \phi_{tt} - \nabla^2 \phi \right) = 0, \quad (2)$$

where the Laplacian assumes the form,

$$\nabla^2 = \frac{1}{r^{n-1}} \frac{\partial}{\partial r} r^{n-1} \frac{\partial}{\partial r}, \quad (3)$$

with $n = 1, 2$, and 3 for plane, cylindrical, and spherical waves, respectively. In equation (2), a_f and a_e denote the frozen and equilibrium sound speeds evaluated at the undisturbed state, respectively. It is convenient to

characterize the medium by an equation of state giving the enthalpy h as a function of p , ρ , and q . It follows that (Broer, 1958)

$$a_f^2 \equiv \left(\frac{\partial p}{\partial \rho} \right)_{s,q} = - \frac{\frac{\partial h}{\partial \rho}}{\frac{\partial h}{\partial p} - \frac{1}{\rho}}, \quad (4)$$

and

$$a_e^2 \equiv \left(\frac{\partial p}{\partial \rho} \right)_{s,q=q} = - \frac{\frac{\partial h}{\partial \rho} + \frac{\partial h}{\partial q} \frac{\partial \bar{q}}{\partial \rho}}{\frac{\partial h}{\partial p} + \frac{\partial h}{\partial q} \frac{\partial \bar{q}}{\partial p} - \frac{1}{\rho}}. \quad (5)$$

Furthermore it can be shown from considerations of thermodynamic stability that $a_f > a_e$. The relaxation time of the single nonequilibrium process is, by definition,

$$\tau_o = - \frac{\tau}{\frac{\partial L}{\partial q} \frac{\partial h}{\partial \rho} + \frac{\partial h}{\partial q} \frac{\partial \bar{q}}{\partial \rho}}, \quad (6)$$

where τ is related to the specific rate process under discussion. The limiting sound speeds of equations (4) and (5) also arise in Einstein's treatment of reacting gases (1920) as the limits of the acoustic velocity for the high and low frequencies. The characteristics of equation (2) are

$$\frac{dr}{dt} = \pm a_f ; 0, \quad (7)$$

as previously shown by Broer (1950); Brinkley & Richardson (1953); and, Wood & Kirkwood (1957), for variants of the wave equation under discussion. For steady disturbances in a medium moving with a velocity, U ,

we replace $\partial/\partial t$ in equation (2) by $U\partial/\partial x$ and find (Vincenti, 1959; Moore & Gibson, 1960),

$$U\tau_0 [(M_f^2-1)\frac{\partial^2}{\partial x^2} - (\frac{\partial^2}{\partial y^2} + \frac{\partial^2}{\partial z^2})]\phi + [(M_e^2-1)\frac{\partial^2}{\partial x^2} - (\frac{\partial^2}{\partial y^2} + \frac{\partial^2}{\partial z^2})]\phi = 0, \quad (8)$$

where the frozen and equilibrium Mach numbers are defined by $M_f \equiv U/a_f$ and $M_e \equiv U/a_e$, respectively. Comparing equations (2) and (8), the following identifications are evident: t corresponds to x , a_f to $1/\sqrt{M_f^2-1}$, a_e to $1/\sqrt{M_e^2-1}$, and τ_0 to $U\tau_0$. Once ϕ is known, the velocity, pressure, and density fields can be calculated from

$$\vec{u}' = \nabla\phi, \quad p' = -\rho_0 \frac{\partial\phi}{\partial t}, \quad \text{and} \quad \frac{\partial\rho'}{\partial t} = -\rho_0 \nabla^2\phi, \quad (9)$$

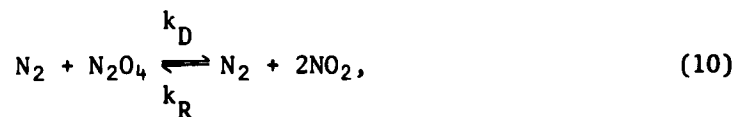
where $\frac{\partial}{\partial t}$ is to be replaced by $U\frac{\partial}{\partial x}$ in steady flow. Finally, if we set $\tau_0 \equiv 0$, or ∞ , in equations (2) and (8), we recover the wave equation of acoustics and the Prandtl-Glauert equation for equilibrium or frozen flow, respectively.

Inspection of these third order equations using Whitham's analysis (1959) reveals that weak disturbances propagate initially with the frozen sound speed along the characteristic direction given by equation (7). Furthermore, these weak waves are expected to decay with distance from the origin both by the usual geometric wave decay found for cylindrical and spherical waves; and, also, by an exponential decay occasioned by the relaxation process for all three geometries of the flow field. Moore & Gibson (1960) indicated the form of the decay for plane waves in relaxing steady flow; Wegener & Cole (1962) provided a complete solution for the system to be discussed later and showed

experimentally that in steady, supersonic flow of a reacting gas mixture, a weak disturbance indeed propagates along the characteristic direction given by the frozen sound speed. The role of the equilibrium sound speed, a_e , and its relation to the wave form at large time (or distance) has been discussed by Chu (1958).

These equations are valid for flows in which all modes but one are in thermodynamic equilibrium, in the sense advanced by Wood & Kirkwood (1957). The rate equation may, therefore, be applied to any nonequilibrium process simply by choosing the progress variable, q , appropriately. Vibrational relaxation, chemical reactions, dissociation, ionization, or electronic excitation--all these rate processes--if present as a single nonequilibrium mode, would fall under the above description.

In this work, equation (2) will first be integrated to yield more general expressions for wave decay. Furthermore, these findings will be tested experimentally, by using a model gas, the well-understood reacting gas mixture,



with which other aspects of nonequilibrium flows have previously been explored (Wegener 1961). As usual, k_D and k_R denote the specific reaction rates for the indicated dissociation and recombination processes, respectively. It will be demonstrated that the predicted

wave decay is experimentally observable. Also, a quantitative determination of wave decay of conical waves will be shown which provides another technique to find relaxation times of fast non-equilibrium processes (Wegener 1964).

2. Analysis of the decay of weak waves

An analytical study of the decay of cylindrical and spherical wave fronts can be carried out in much the same way as that for plane waves (Wegener & Cole 1962). Let us first introduce the characteristic coordinates:

$$\xi = t - \frac{r}{a_f}, \quad \eta = t + \frac{r}{a_f} \quad (11)$$

so that

$$\frac{\partial}{\partial t} = \frac{\partial}{\partial \xi} + \frac{\partial}{\partial \eta}, \quad \frac{\partial}{\partial r} = -\frac{1}{a_f} \left(\frac{\partial}{\partial \xi} - \frac{\partial}{\partial \eta} \right). \quad (12)$$

From equation (9), we conclude:

$$p' = -\rho_0(\phi_\xi + \phi_\eta), \quad u'_r = -\frac{1}{a_f}(\phi_\xi - \phi_\eta), \quad (13)$$

when $\phi_\xi = \partial\phi/\partial\xi$, $\phi_\eta = \partial\phi/\partial\eta$ and u'_r denotes the radial velocity. Now the basic equations (2) and (3) can be rewritten in the form

$$\left(\frac{\partial}{\partial t} + \frac{1}{\tau_0}\right) \left(\frac{1}{a_f^2} \frac{\partial^2}{\partial t^2} - \frac{\partial^2}{\partial r^2} - \frac{n-1}{r} \frac{\partial}{\partial r}\right) \phi + \frac{1}{\tau_0} \left(\frac{1}{a_e^2} - \frac{1}{a_f^2}\right) \frac{\partial^2 \phi}{\partial t^2} = 0, \quad (14)$$

and substituting equation (12) into equation (14), we have

$$\left(\frac{\partial}{\partial \xi} + \frac{\partial}{\partial \eta} + \frac{1}{\tau_0}\right) \left\{ \frac{4}{a_f^2} \frac{\partial^2}{\partial \xi \partial \eta} + \frac{n-1}{r} \frac{1}{a_f} \left(\frac{\partial}{\partial \xi} - \frac{\partial}{\partial \eta} \right) \right\} \phi + \frac{1}{\tau_0} \left(\frac{1}{a_e^2} - \frac{1}{a_f^2} \right) \left(\frac{\partial}{\partial \xi} + \frac{\partial}{\partial \eta} \right)^2 \phi = 0. \quad (15)$$

Equation (15), like equation (2), possesses a 3-fold continuum of characteristics. A wave front is defined here as that characteristic across which ϕ is continuous, while the normal derivatives of ϕ and, therefore, all physical variables, undergo discontinuous changes. Hence, if $\xi = \xi_0$ is a wave front, $\frac{\partial \phi}{\partial \xi}$ is discontinuous across the wave front, while ϕ , $\partial \phi / \partial \eta$, $\partial^2 \phi / \partial \eta^2$ are all continuous. Keeping these remarks in mind, we can integrate equation (15) with respect to ξ from $\xi = \xi_0 - \epsilon$ to $\xi = \xi_0 + \epsilon$, and then let $\epsilon \rightarrow 0$. All terms that are continuous at $\xi = \xi_0$ will drop out as $\epsilon \rightarrow 0$, leaving only the following terms:

$$\frac{4}{a_f^2} \frac{\partial}{\partial \eta} [\phi_\xi] + \left\{ \frac{n-1}{r} \frac{1}{a_f} + \frac{1}{\tau_0} \left(\frac{1}{a_e^2} - \frac{1}{a_f^2} \right) \right\} [\phi_\xi] = 0, \quad (16)$$

where the square bracket identifies a jump of whatever quantity appears in the bracket, across the characteristic. Now

$$[\phi_\eta] = 0, \quad \frac{\partial}{\partial \eta} [\phi_\eta] = 0. \quad (17)$$

It follows from equations (13), (16), and (17) that

$$\frac{\partial}{\partial \eta} [p'] + \left\{ \frac{n-1}{2} \frac{1}{\eta - \xi_0} + \frac{1}{4\tau_0} \left(\frac{a_f^2}{a_e^2} - 1 \right) \right\} [p'] = 0. \quad (18)$$

This equation can be readily integrated to give

$$[p'] = \text{const } r^{-\frac{n-1}{2}} \exp(-Ar) \quad (19)$$

where

$$A = \frac{1}{2a_f \tau_0} \left(\frac{a_f^2}{a_e^2} - 1 \right). \quad (20)$$

Similar expressions hold for u'_r and ρ' .

For a medium with a number of nonequilibrium processes, the wave front will still decay as

$$r^{-\frac{n-1}{2}} \exp(-r/\lambda) \quad (21)$$

except that the relaxation length, λ , is given by a more complex formula.

Let us next consider the decay of a stationary wave front in steady supersonic flow. Since the governing equation (8) has exactly the same structure as equation (2), the decay law can be written down immediately. First, we introduce the quantity

$$A' = \frac{1}{2U_{\tau_0}/\sqrt{M_f^2-1}} \left[\left(\frac{1/\sqrt{M_f^2-1}}{1/\sqrt{M_e^2-1}} \right)^2 - 1 \right] = \frac{M_e^2 - M_f^2}{2U_{\tau_0} \sqrt{M_f^2-1}} \quad (22)$$

and redefine n and r for stationary wave fronts as follows:

1. Two-dimensional steady supersonic flow: $n = 1$ and $r = y$ --plane stationary wave fronts.
2. Axially symmetric steady supersonic flow: $n = 2$ and $r = \sqrt{y^2+z^2}$ --conical wave fronts.

The discontinuous changes in density and other flow variables will then follow the decay law

$$[\rho'] = \text{const } r^{-\frac{n-1}{2}} \exp(-A'r), \quad (23)$$

etc.

For $n = 1$, we reproduce the result of Wegener and Cole (1958).

The ratio of A' and A is

$$\frac{A'}{A} = (1 - 1/M_f^2)^{-\frac{1}{2}}. \quad (24)$$

It is always greater than 1 and approaches 1 monotonically as $M_f \rightarrow \infty$, as shown in figure 1. It is seen that above Mach numbers of about three, $A \approx A'$ for all practical purposes.

3. Properties of the model gas mixture

The thermodynamic properties of the gas mixture of equation (10) as reviewed by Gray & Yoffe (1955) are well-known at equilibrium. From the results of shock tube experiments (Carrington & Davidson 1953) and nonequilibrium nozzle flow experiments (Wegener 1958), it is reasonable to assume a reaction mechanism given by

$$\left[\frac{\partial (N_2O_4)}{\partial t} \right]_T = k_R (NO_2)^2 (N_2) - k_D (N_2O_4) (N_2). \quad (25)$$

For reactant mole fractions up to $n_R = 0.05$, the recombination rate constant of equation (25), $k_R = 3 \times 10^{14} \text{ cm}^6/(\text{mole}^2 \text{ sec})$, was found around room temperature. Equation (25) may, in addition, be cast in the form of the rate law (1), or (1'). Working with mass fractions, $\omega_i = m_i/m$, we can identify the progress variable by $q \equiv \omega_{N_2O_4}$. This designation determines the state uniquely, because the nitrogen mass fraction remains unchanged and the reactant mass fractions are known initially at equilibrium. With the equilibrium constant in terms of pressure

$$K_p(T) = p^* e^{-\frac{T^*}{T}}, \quad (26)$$

where $p^* = 1.538 \times 10^8$ atmospheres and $T^* = 6882$ °K (Strehlow, 1964) and recalling that $K_p = (k_D/k_R)RT$, we find for the L-function of equation (1)

$$L(p, \rho, q) = (1 - \omega_{N_2} - q)^2 - \frac{K_p(T)}{4p} q(\Omega - q), \quad (27)$$

where

$$\Omega = \frac{\mu_{N_2 O_4}}{\mu_{N_2}} \omega_{N_2} + 2(1 - \omega_{N_2}) \quad (28)$$

with μ_i , the molecular weight. Furthermore,

$$\tau = \frac{\mu_{N_2} \mu_{NO_2}}{2k_R \rho^2 \omega_{N_2}}. \quad (29)$$

For fixed ω_{N_2} we see that $\Omega = \text{constant}$; and, if we set $L \equiv 0$, we recover the law of mass action. τ_0 in equation (2) may be computed immediately from equations (6) and (29).

The partial derivatives entering equations (4) to (6) have previously been given for this system by Wegener & Cole (1962) as their equations (31) to (36). Typical values of these parameters at equilibrium and atmospheric pressure and temperature as obtained on a digital computer are shown in figure 2. Values are given as a function of reactant mole fraction, n_R ; and, the derivatives have been made dimensionless by appropriate variables chosen for pure nitrogen at NTP. Also given is the square of the ratio of the limiting sound speeds and the degree of dissociation at equilibrium, $\bar{\alpha}$, of the reactants only. The

sound speeds are close to each other; and, it is interesting to note that their difference reaches a maximum of about 8% of a_e at $n_R = 0.14$.

4. Experimental techniques

Experiments on propagation of weak waves were carried out in a small firing range filled with the model gas mixture of equation (10). Standard projectiles of about 0.22-inch diameter were fired from a commercial Winchester 220 Swift rifle at about 1220 m/sec, or $M = 3.6$. The bullets traversed a test box with two circular optical glass windows of 13-inch diameter, spaced about 1.5 inches apart. With bullet entry and exit holes having been sealed with plastic diaphragms, the cleaned box was pumped out and then filled with the carefully prepared dry gas mixture at known temperature, total pressure and reactant partial pressure. A fume hood was placed above the test box to exhaust the reactants after the shot had pierced the seals.

With parallel light incident at a right angle to the bullet path, a shadowgraph of the projectile was taken in the box with a 1/2-microsecond exposure of a 10 KV spark unit. An 8x10-inch film (or plate) holder was located adjacent to one window. To insure dimensional accuracy comparisons of a grid of known dimensions, photographed simultaneously, were made with pictures taken with glass plates. A second similar spark shadowgraph station was located in free air about 75 cm downstream to record a second photograph. Fiducial marks of known distance appeared in both photographs and the elapsed time between the release of the two sparks was measured. Since the

speed reduction of the projectile between the two stations was found to be negligible ($c_D = 0.37$ with a bullet mass of 48 grams,) the speed of the projectile could be determined directly to better than 1%.

The bow shock wave of the bullet was used as a constant speed disturbance generator, as seen in the upper shadowgraph of figure 3 taken in non-reacting air. 1/8-inch thick metal strips divided the box on both sides of the flight path. (The black strips visible in the photographs are seals.) In each divider-strip were drilled, on the centerlines, a line of small holes parallel to the flight path. The holes in the upper strip were spaced 1 inch apart; the lower divider holes 0.04-inch apart between centers.

With the strong bow wave sweeping across both sets of holes, the increased pressure behind the shock produces a succession of gas puffs through the holes. These, in turn, generate individual, weak spherical waves on the far side of the divider. Vortices may also be noted in the photographs. These weak waves are the object of our experiments. The classical Mach cone is formed by the waves running together on the side with the many holes. Succeeding the initial disturbance, there follows a complicated pressure-time history of the flow field of the bullet, to which the holes in the divider plates are being exposed. Since, clearly, the initial disturbance, made visible by changes of index of refraction of the gas, cannot be of vanishing strength, and considering the non-uniform succeeding flow,

it is expected that the waves produced have nonlinear components. However, as will be demonstrated, the technique described yielded wave patterns both in non-reacting air and also in the reacting model gas mixture, which were suitable for comparison with the theoretical results from linear theory.

5. Results and discussion

The properties of equation (23) were studied by determining the decay of weak conical and spherical waves from shadowgraphs, such as those shown in figures 3 and 4. These photographs were taken at thermodynamic states close to those shown in figure 2. However, the reactant mole fractions selected for the experiments did not exceed $n_R = 0.15$, since at higher concentrations the mechanism and rate of the reaction become increasingly doubtful, and owing to the reddish-brown color of nitrogen dioxide, the gas mixture becomes practically opaque. Typical experimental conditions are listed in table I, and the results in the figures are identified by numbers corresponding to this table. The temperature and total pressure were, in each instance, close to the average values indicated; however, properties were computed separately for the exact conditions of each experiment. The calculations included theoretical predictions of the relaxation time, and the term A' of equation (22), both based on $k_R = 3 \times 10^{14} \text{ cm}^6/(\text{mole}^2 \text{ sec})$. The two groups of experiments listed in table I differ in the choice of the hole size in the divider strips used for the production of the disturbances. For greater clarity all photographs shown here were

taken with an 1/8-inch hole yielding the stronger initial disturbances.

Since shadowgraphs may be interpreted in terms of change of index of refraction occasioned by a density change in the medium under observation, we will characterize the strength of the wave front by a dimensionless jump in density defined by $\Delta\rho/\rho_0 \equiv (\rho - \rho_0)/\rho_0$ where ρ is the density immediately behind the disturbance, and ρ_0 the density in the undisturbed medium. Such density jumps may be introduced in equation (23). However, before proceeding, we note that for $r = 0$, i.e., at the origin of the disturbance, we have a singularity for $n = 2, 3$. This is to be expected from previous encounters with this problem in slender body theory. Choosing some distance, r , downstream from the origin of the disturbance, and assuming that the linearized equations are applicable, if $r \geq U\tau_0$, where $U\tau_0$ is a relaxation length, we may now rewrite equation (23) to obtain

$$\frac{\Delta\rho}{(\Delta\rho)_1} = \left(\frac{r}{r_1}\right)^{-\frac{n-1}{2}} e^{-A'(r-r_1)}, \quad (30)$$

where A' takes the form appropriate to the problem under study and the left-hand side is the ratio of two density jumps. The decay in wave strength as a function of distance expected from equation (30) for all three geometries and for a typical experimental situation with $A = A' = 1 \text{ cm}^{-1}$ (or $\tau_0 = 2.5 \text{ } \mu\text{sec}$) is shown in figure 5.

Results of disturbance decay or decrease of $\Delta\rho$ with r will next be investigated by two different techniques to be applied to our

experiments. At first, we assume that equation (30) is directly applicable by neglecting the effects of nonlinearity discussed in the last section. The conical waves in the steady flow depicted in figures 3 and 4 correspond to unsteady cylindrical waves with $n = 2$. Inspection of the lower photograph in figure 3 and the shadowgraphs of conical disturbances shown in figure 4 clearly shows that for increasing reactant mole fraction, i.e., decreasing relaxation time, the conical disturbance disappears at decreasingly shorter distances from the origin. This qualitative observation was checked by increasing the film sensitivity with increasing reactant mole fraction to obtain a uniformly illuminated background for the undisturbed reacting mixture. The upper photograph in figure 3 reveals that in non-reacting air, no decay of the conical wave is readily observable from the apparent strength of the density jump within the scale of this experiment. In an additional series of experiments in non-reacting air this persistence of the conical disturbances was still noted with gray filters interspersed in the light beam and corresponding to the absorption of the reactants.

Secondly, the photographs with relaxation reveal that, as predicted by equation (30), spherical disturbances ($n = 3$) decay more rapidly than the conical ones ($n = 2$), all other conditions being equal. In fact, in the air shot of figure 3, we find spherical and conical disturbances visible in the entire flow field while in the lower picture of the relaxing mixture, the spherical disturbances have disappeared at distances r where the conical one is still visible. In addition to

these qualitative observations, the conical wave decay may be determined roughly by a crude visual estimate of the disappearance of the disturbance in equally-treated positives of the shadowgraphs. We may rearrange equation (30) to have

$$A'r_1 = \frac{1}{\frac{r}{r_1} - 1} \left[\ln \frac{(\Delta\rho)_1}{\Delta\rho} - \frac{1}{2} \ln \frac{r}{r_1} \right]. \quad (31)$$

It is possible to estimate from the photograph a value of the distance along the conical disturbance from the origin where the conical disturbance disappears to the eye. Calling this distance s , a corresponding value of the coordinate, r , is given by $r = s/M_f$. Considering the sensitivity to light of the photographic material one may rather arbitrarily assign values of $(\Delta\rho)_1/\Delta\rho = 10$ and 50 to the location where the trace disappears on the positive with $(\Delta\rho)_1$ taken to be at $r = 1$ cm. Getting the value of r at extinction of the trace we may then compute two corresponding values of A from equation (31) as shown on figure 6 for the experiments listed in table 1 and a number of additional unlisted experiments. Predicted relaxation time rather than measured mole fraction is shown on the abscissa. The results scatter about the predicted values of A and calculations reveal that the estimated vanishing point of the disturbance on the positives occurs somewhere at $(\Delta\rho)_1/\Delta\rho = 30$. Since A is lineally related to relaxation time, or rate constant, these may be computed directly from such results. This simple method of estimating relaxation time may prove useful in application to unknown systems in order to provide an initial hint of the

order of magnitude of rate of processes. Unfortunately, similar attempts to measure the wave strength of the spherical waves quantitatively have failed.

Next, we turn to a more detailed evaluation of the decay of the conical waves. By measuring the angle of the conical wave as a function of r , the results shown in figure 7 are found. It is noted that the wave angle decreases slightly with r in air and the reacting mixture. This bending or wave decay has two causes: for one, we expect a geometrical wave decay even for non-reacting air. We see that the exponential relaxation term in equation (30) for frozen flow with $\tau_0 = \infty$ and $A = 0$ yields one. Such behavior of wave decay of the conical wave with $n = 2$ is in contrast to that of the non-decaying shock wave of a slender cone. The reason for this difference is found because the disturbance generation by the bow shock of the bullet consists of a rapid succession of (hopefully) rather sharply defined, finite puffs of air coming from the holes in the divider, in direct analogy to the single unsteady cylindrical wave pulse. Non-linearities, in addition, arise from the initial shock and succeeding pressure field, as seen in figure 3 and discussed previously. (It appears that viscous damping is practically negligible at distances r of our experiments.) In order to "calibrate" all non-linear effects lumped together we may first write equation (23) in terms of the density jump by

$$\ln\left(\frac{\Delta\rho}{\rho_0} r^{1/2}\right) = -A'r + \text{constant} \quad (32)$$

to separate geometrical and relaxation decay. For frozen flow with $A' = 0$, the right-hand side will give a constant whose value depends on the initial wave strength. By assuming the weak shock to be locally two-dimensional, the density jump may generally be computed from the angle measurements by

$$\frac{\Delta \rho}{\rho_0} = \frac{\rho - \rho_0}{\rho_0} = \frac{(\gamma+1) M_f^2 \sin^2 \theta}{(\gamma-1) M_f^2 \sin^2 \theta + 2} - 1, \quad (33)$$

where θ is the shock angle. In our process, the reacting flow remains frozen across the disturbance; γ , the ratio of the specific heats, applies to the mixture, and $M_f = M$ for air. Experimental results on wave strength as a function of r are given in figure 8, plotted as suggested by equation (32). At first, we observe from figures 7 and 8 that the initial wave strengths of the experiments of group 2 with the larger holes are indeed higher, as expected. Furthermore, we see that the decaying waves approach the frozen Mach angle as computed independently at large r . In fact, the frozen Mach angle is practically attained where the wave ceases to be visible. For the relaxing flow this represents additional experimental evidence that weak disturbances indeed propagate at the frozen sound speed. On the other hand, we see that for non-reacting air with $A' = 0$, we do not observe $\ln[(\Delta \rho / \rho_0) r^{1/2}] = \text{constant}$, as expected from equation (32). We find empirically a decay as approximated by the dashed lines in the semilog graphs of figure 8; and, we ascribe this decay to all the nonlinear effects lumped together. Since the experiments with the reacting gas mixture were carried out at

practically the same Mach numbers and Reynolds numbers, we propose to assume that the nonlinear flow-field effects found quantitatively for air are also equal in magnitude with the relaxation process being present. In this manner a decay calibration for non-linearity as a function of r becomes available from the air pictures. After subtracting this fortunately small correction, the chemical damping factor, A' , may be directly found from the slope of the straight lines of the other experiments in figure 8. This final result is shown in figure 9, where A' has again been plotted versus relaxation time, and the agreement with the predicted values is satisfactory. The agreement is found for both hole sizes and therefore initially different wave strengths. This fact appears to imply that the correction procedure used is valid.

In conclusion it is seen that relaxation times may be found by quantitative observation of the decay of weak conical waves in a relaxing flow field. The linearized equations can be applied to experiments with a small correction accounting for the initial finite wave strength. It is suggested that these findings may be applied to the study of unknown relaxation processes.

REFERENCES

- Brinkley, Jr., S. R. & Richardson, J. M. 1953 On the structure of plane detonation waves with finite reaction velocity. Fourth Symposium (International) on Combustion, The Williams and Wilkins Co., Baltimore, Md.
- Broer, L. J. F. 1950 On the influence of acoustic relaxation on compressible flow. *Appl. Sci. Res. A*, 2, 447.
- Broer, L. J. F. 1958 Characteristics of the equations of motion of a reacting gas. *J. Fluid Mech.* 4, 276.
- Carrington, T. & Davidson, N. 1953 Shock waves in chemical kinetics: The rate of dissociation of N_2O_4 . *J. Phys. Chem.* 57, 418.
- Chu, B. T. 1958 Wave propagation in a reacting mixture. *Heat Transfer & Fluid Mech. Inst.* 80.
- Clarke, J. F. & McChesney, M. 1964 The Dynamics of Real Gases, Butterworths, Washington, p. 186.
- Einstein, A. 1920 Schallgeschwindigkeit in teilweise dissoziierten Gasen. Sitzungsberichte d. preussischen Adak. d. Wiss. Wien, 18, 380.
- Gray, P. & Yoffe, A. D. 1955 The reactivity and structure of nitrogen dioxide. *Chem. Rev.* 55, 1069.

Kirkwood, J. G. & Wood, W. W. 1957 Hydrodynamics of a reacting and relaxing fluid. J. Appl. Phys. 28, 395.

Moore, F. K. 1958 Propagation of weak waves in a dissociated gas. J. Aero/Space Sci. 25, 279.

Moore, F. K. & Gibson, W. E. 1960 Propagation of weak disturbances in a gas subject to relaxation effects. J. Aero/Space Sci. 27, 117.

Strehlow, R. A. 1964 Private communication.

Vincenti, W. G. 1959 Non-equilibrium flow over a wavy wall. J. Fluid Mech. 6, 481.

Wegener, P. P. 1958 Measurement of rate constants of fast reactions in a supersonic nozzle. J. Chem. Phys. 28, 724.

Wegener, P. P. 1961 A review of investigations of stationary supersonic nozzle flow with a reacting gas mixture. "Combustion - and Propulsion" - Fourth AGARD Colloquium, Pergamon Press.

Wegener, P. P. & Cole, J. D. 1962 Experiments on propagation of weak disturbances in stationary supersonic nozzle flow of chemically reacting gas mixtures. Eighth Symposium (International on Combustion, The William & Wilkins Co., Baltimore, Md.

Wegener, P. P. 1964 Determination of reaction rates from measurements of the decay of weak disturbances. J. Chem. Phys. 41, 1512.

Whitham, G. B. 1959 Some comments on wave propagation and shock wave structure with application to magnetohydrodynamics. Comm. Pure Appl. Math. 12, 113.

n_R	Experiment Number	U (m/sec)	M_f	M_e	A' (cm^{-1})	τ (μsec)	U_τ (cm)
0	137	1230	3.57	--	0	∞	∞
0.026	145	1230	3.57	3.70	0.16	6.93	.852
0.045	142	1230	3.55	3.75	0.38	4.52	.547
0.054	146	1230	3.64	3.86	0.48	3.82	.470
0.081	143	1230	3.70	3.96	0.88	2.58	.317
0.101	144	1230	3.76	4.04	1.13	2.20	.271
0.152	147	1230	3.93	4.24	1.86	1.43	.176

Remarks: 1/32-inch holes; average $T = 296^\circ\text{K}$; average $p = 1.01$ atmos.

0	149	1230	3.55	--	0	∞	∞
0	155	1230	3.59	--	0	∞	∞
0.053	150	1240	3.66	3.88	0.50	3.77	.467
0.054	158	1220	3.60	3.82	0.49	3.98	.486
0.074	154	1220	3.67	3.93	0.74	3.06	.373
0.099	151	1220	3.71	3.98	1.20	1.98	.242
0.123	156	1190	3.72	4.07	1.38	1.89	.225
0.152	157	1220	3.90	4.20	1.72	1.56	.190

Remarks: 1/8-inch holes; average $T = 296^\circ\text{K}$; average $p = 1.0$ atmos.

NOTE: The values of A' , τ , and U_τ given are predictions based on $k_R = 3 \times 10^{14} \text{cm}^6/(\text{moles}^2 \text{sec})$.

TABLE 1: EXPERIMENTAL ENVIRONMENT AND THEORETICALLY PREDICTED QUANTITIES.

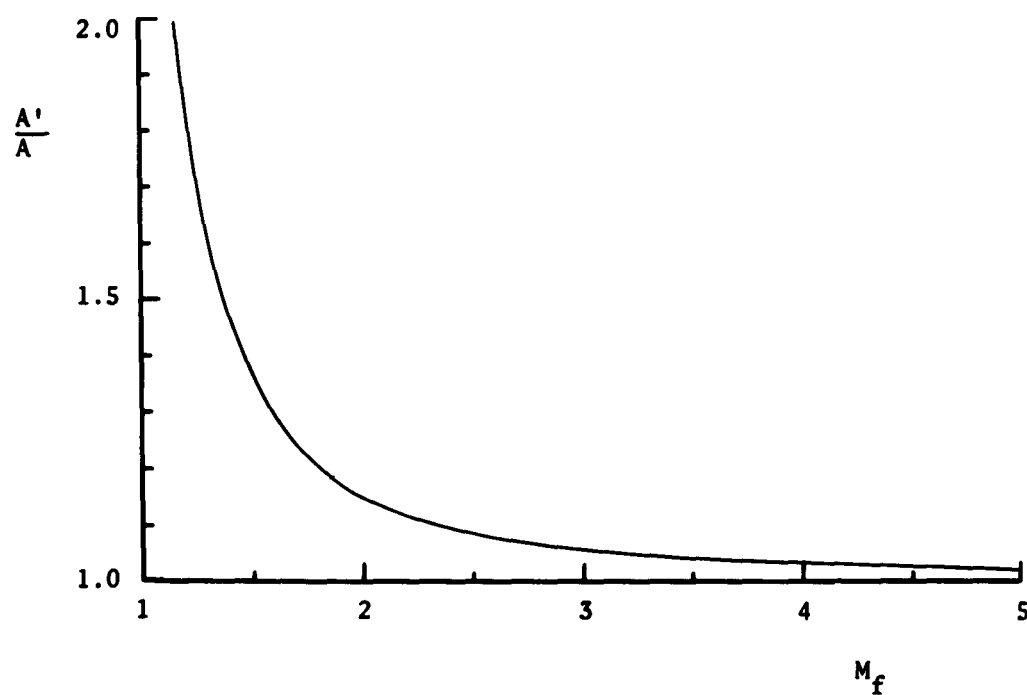


FIGURE 1: Ratio of the chemical damping terms for steady and unsteady flow as a function of frozen Mach number.

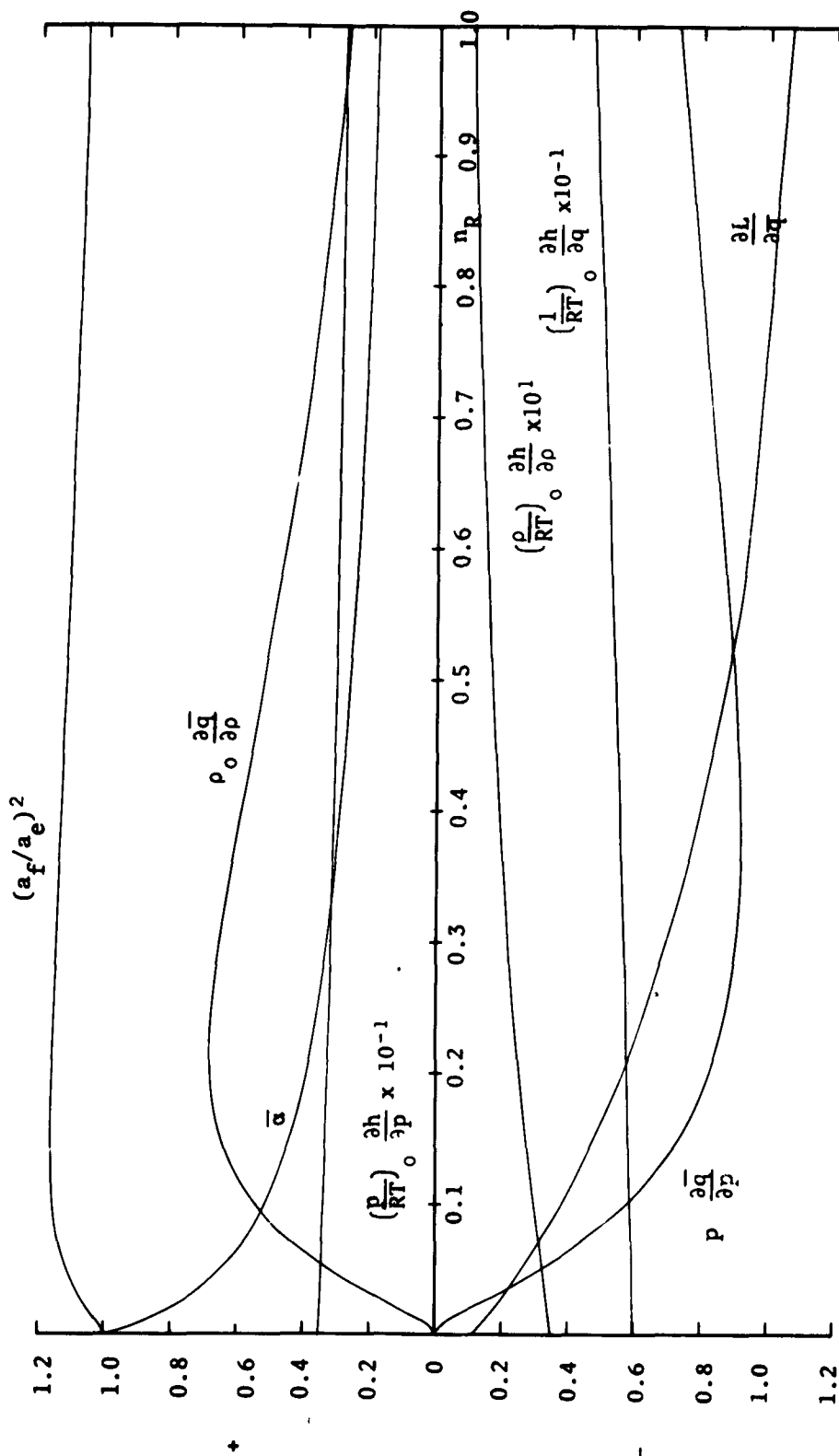


FIGURE 2: Partial derivatives, sound speeds and degree of dissociation at equilibrium as a function of reactant mole fraction, n_R .

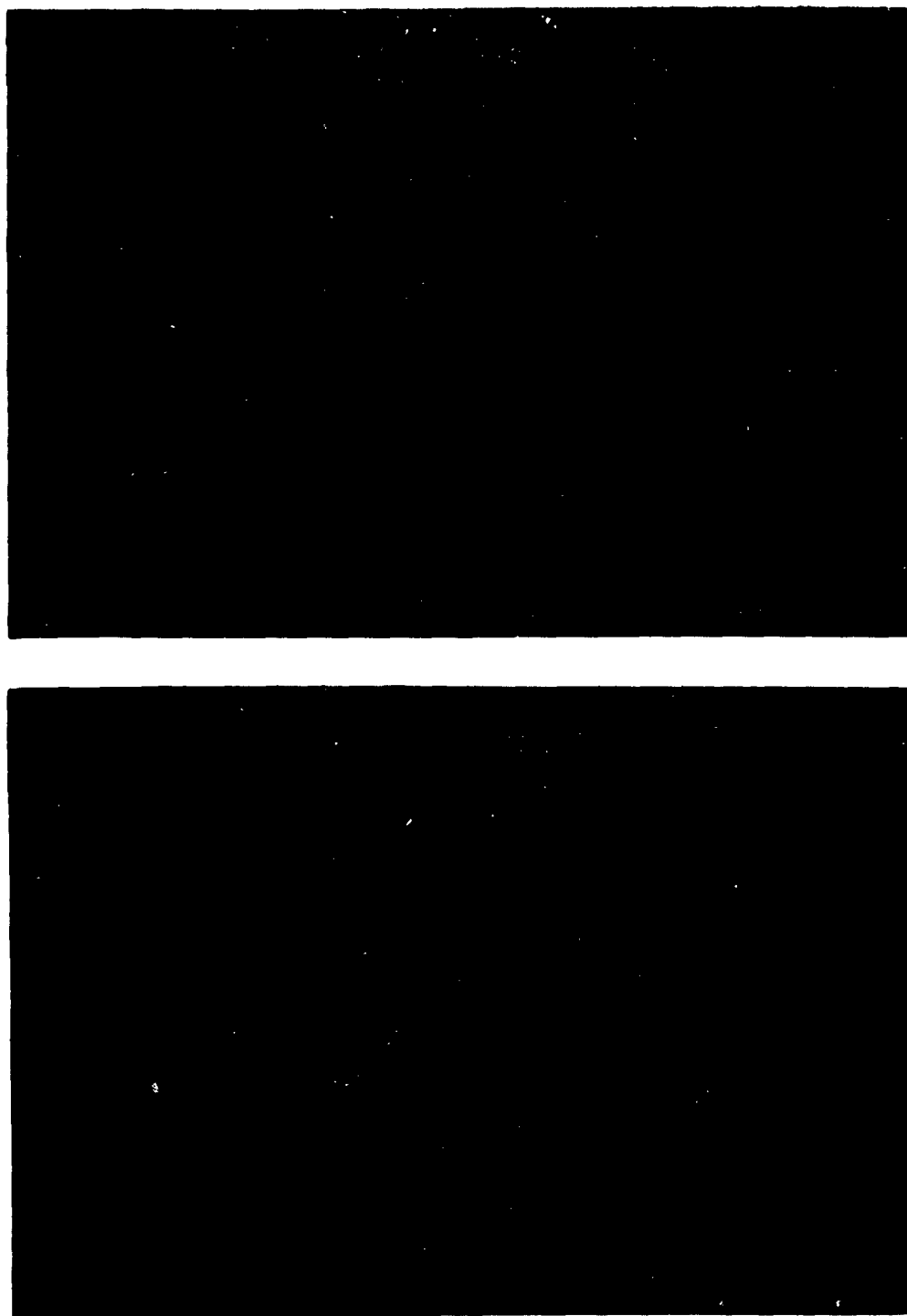


FIGURE 3: Firing range shadowgraphs - Upper figure, air, experiment 155; lower figure, reacting gas mixture, experiment 156 (see table I)



n_R	Exp.
-------	------

0(air)	155
--------	-----

0.054	158
-------	-----

0.123	156
-------	-----

0.152	157
-------	-----

FIGURE 4: Shadowgraphs of weak conical disturbances for the indicated reactant concentrations at a mean $M_f = 3.7$ at NTP.

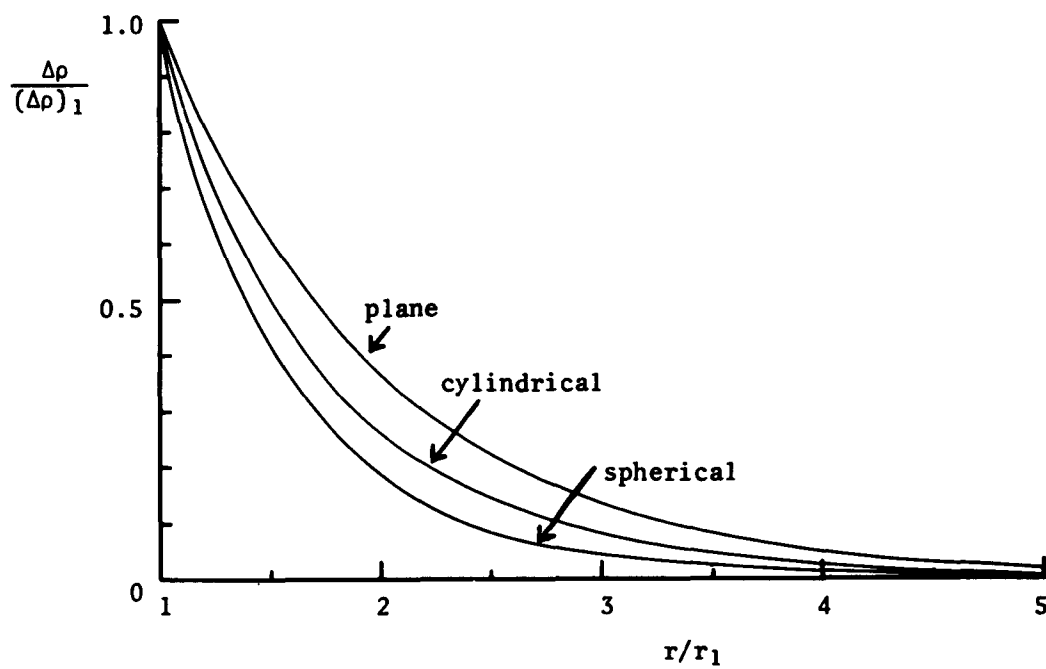


FIGURE 5: Theoretical decay of weak plane, conical and spherical waves for $A = A' = 1 \text{ cm}^{-1}$ ($\tau_0 = 2.5 \text{ } \mu\text{sec}$) and $r_1 = 1 \text{ cm}$.

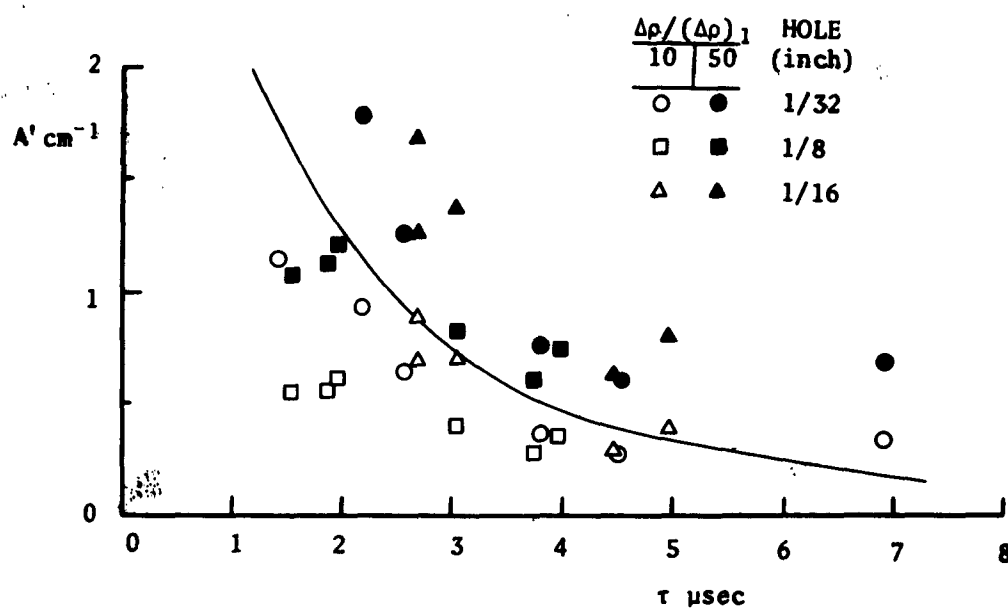


FIGURE 6: Comparison of predicted and measured chemical damping terms, A' , from estimates of visual disappearance of conical wave decay.

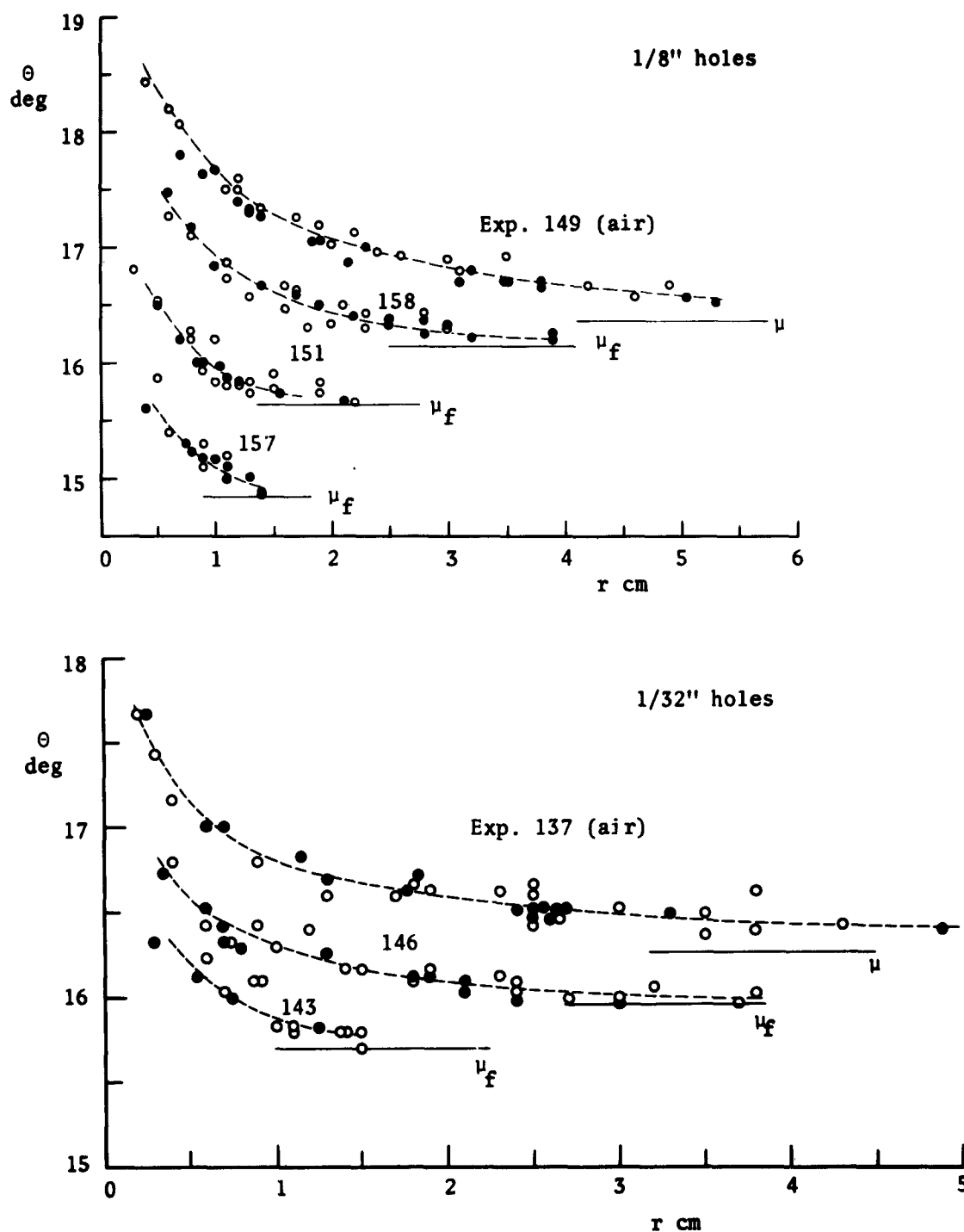


FIGURE 7: Angle of weak conical waves as found by independent observers indicated by \circ and \bullet .

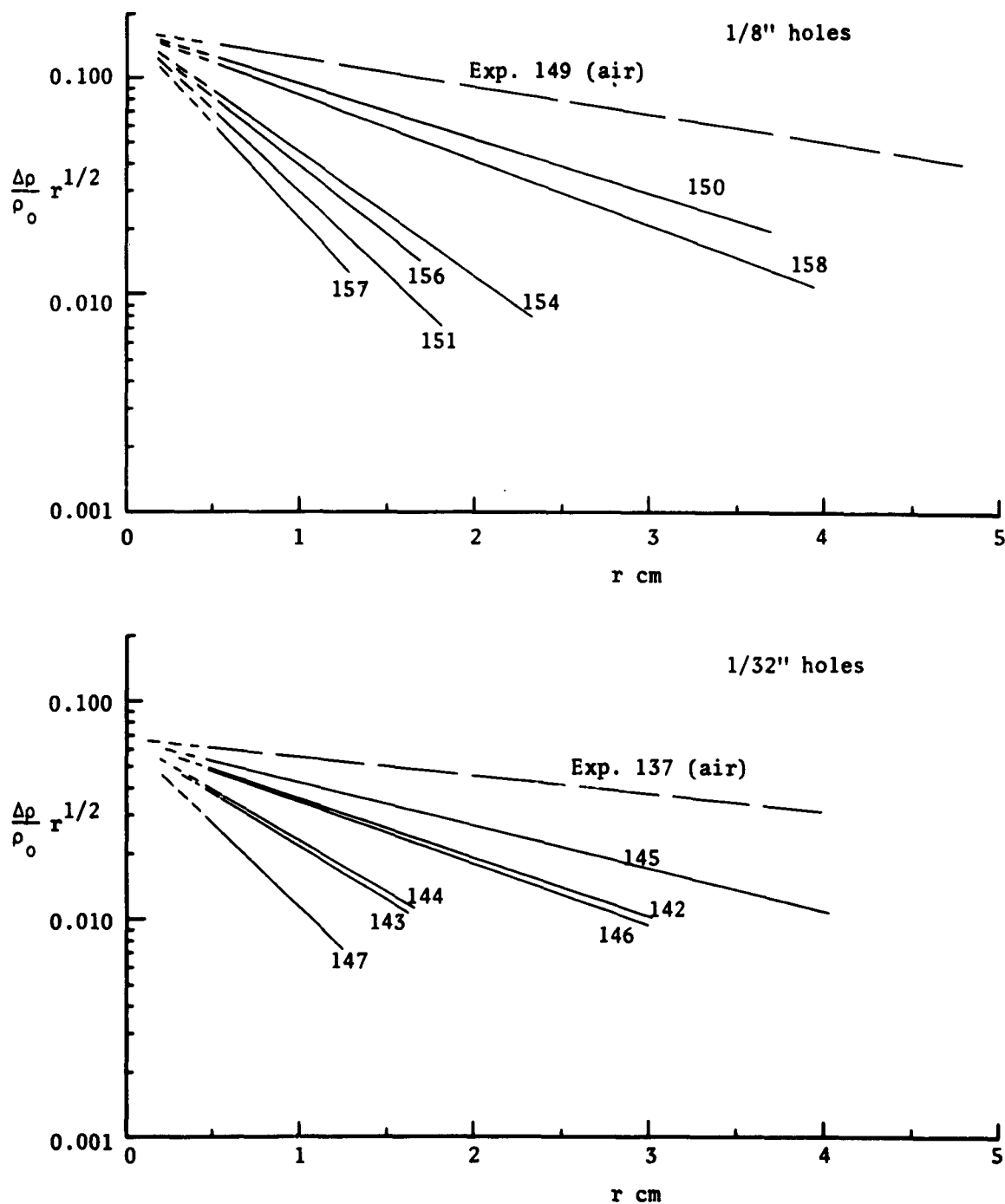


FIGURE 8: Conical wave strength as a function of r computed from the wave angle.

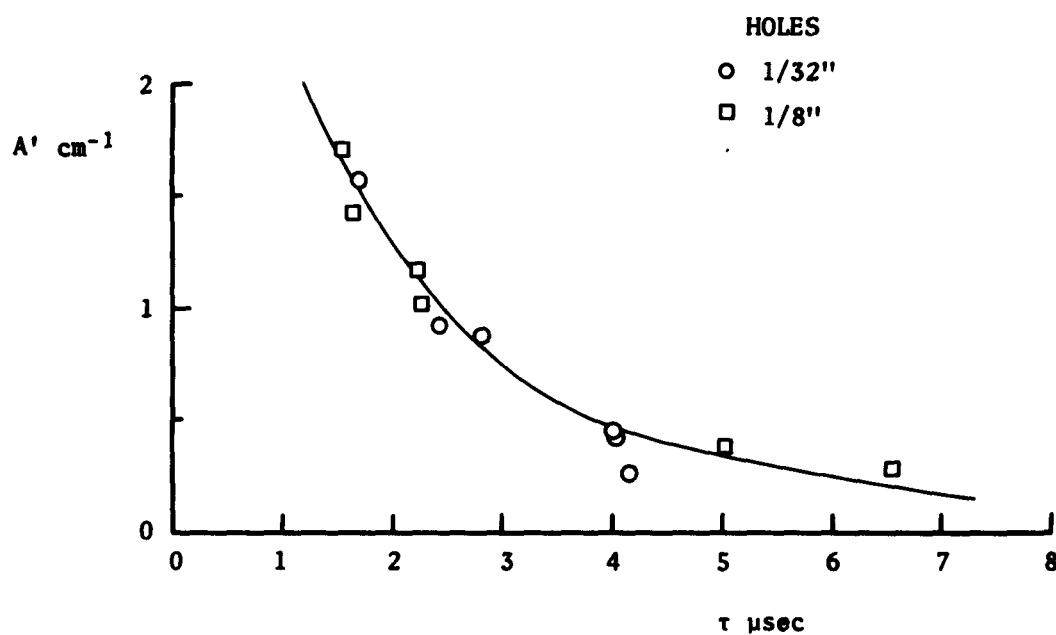


FIGURE 9: Comparison of predicted and measured chemical damping term A' from slope measurements of conical wave decay.